Morphology and composition of particles emitted from a port fuel injection gasoline vehicle under real-world driving test cycles

Jiaoping Xing[1], Longyi Shao[1,*], Wenbin Zhang[2], Jianfei Peng[3], Wenhua Wang[1], Cong Hou[1], Shijin Shuai[2], Min Hu[3], Daizhou Zhang[4,*]

1. State Key Laboratory of Coal Resources and Safe Mining, School of Geoscience and Survey Engineering, China University of Mining and Technology (Beijing), Beijing 100083, China. E-mail: xingjiaoping@qq.com
2. State Key Laboratory of Automotive Safety and Energy, Department of Automotive Engineering, Tsinghua University, Beijing 100084, China
3. State Key Joint Laboratory of Environmental Simulation and Pollution Control, College of Environmental Sciences and Engineering, Peking University, Beijing 100871, China
4. Faculty of Environmental and Symbiotic Sciences, Prefectural University of Kumamoto, Kumamoto 862-8502, Japan

ARTICLE INFO

ABSTRACT

Traffic vehicles, many of which are powered by port fuel injection (PFI) engines, are major sources of particulate matter in the urban atmosphere. We studied particles from the emission of a commercial PFI-engine vehicle when it was running under the states of cold start, hot start, hot stabilized running, idle and acceleration, using a transmission electron microscope and an energy-dispersive X-ray detector. Results showed that the particles were mainly composed of organic, soot, and Ca-rich particles, with a small amount of S-rich and metal-containing particles, and displayed a unimodal size distribution with the peak at 600 nm. The emissions were highest under the cold start running state, followed by the hot start, hot stabilized, acceleration, and idle running states. Organic particles under the hot start and hot stabilized running states were higher than those of other running states. Soot particles were highest under the cold start running state. Under the idle running state, the relative number fraction of Ca-rich particles was high although their absolute number was low. These results indicate that PFI-engine vehicles emit substantial primary particles, which favor the formation of secondary aerosols *via* providing reaction sites and reaction catalysts, as well as supplying soot, organic, mineral and metal particles in the size range of the accumulation mode. In addition, the contents of Ca, P, and Zn in organic particles may serve as fingerprints for source apportionment of particles from PFI-engine vehicles.

© 2018 The Research Center for Eco-Environmental Sciences, Chinese Academy of Sciences. Published by Elsevier B.V.

Introduction

Air pollution by particulate matter (PM) is a large concern in populated megacities due to the influence on solar radiation transfer in the atmosphere (Bond et al., 2013; Huang et al., 2014) and the adverse effects on human health (Chart-Asa and Gibson, 2015; Liu et al., 2017; Shao et al., 2017a, 2017b). Recent rapid increase in energy consumption and automobile

---

* Corresponding authors. E-mail: shaoL@cumtb.edu.cn (Longyi Shao), dzzhang@pu-kumamoto.ac.jp (Daizhou Zhang).

manufacturing in developing countries has aggravated the issues of PM pollution. Vehicles are one of the most substantial anthropogenic sources of PM, and the relative contribution of primary particulate matter from traffic to the $PM_{2.5}$ in Beijing can be up to 31% (Yu et al., 2013). Vehicles emit a large amount of PM and gaseous pollutants (Myung and Park, 2012). The total number of vehicles in China reached 269 million in 2015, of which approximately 81% were powered by gasoline engines (National Bureau of Statistics of China, 2015), and most of the gasoline vehicles were equipped with port fuel injection (PFI) engines. It was reported that the market share of PFI-engine vehicles comprised 50% of the new, light-duty fleet in the USA (California Air Resources Board (CARB), 2010).

Recent studies have revealed that the emission and the physical and chemical properties of particles from gasoline engines are dependent on both engine's operating parameters (fuel-to-air equivalence ratio, speed, and load) and fuel injection strategies (homogeneous or stratified mode) (Jakober et al., 2008; Fu et al., 2014; Zhu et al., 2016; S. Chen et al., 2017). The variation of the parameters, such as air-to-fuel ratios and spark timing, affects the in-cylinder temperature, and can directly influence particle formation and growth. Furthermore, fuel quality and composition, such as sulfur and aromatics contents, have been found to influence the emission of PM (Leach et al., 2013; Karavalakis et al., 2015). It has been identified that the total number of nucleation mode particles increases with sulfur content in fuels (Liu et al., 2007). Aromatics, olefins, Methyl-cyclopentadienyl Manganese Tricarbonyl (MMT), ethanol content in the fuel have impacts on the morphologies and elemental compositions of particles from gasoline engines (Xing et al., 2017). A recent study confirmed the importance of PFI-engine vehicles as sources of PM in polluted urban atmospheres, in particular, in the consideration of the emissions according to the number of particles rather than the mass of particles (Arsie et al., 2013). However, the physical and chemical characteristics of particles emitted from PFI engines have not been carefully identified.

The variation of vehicle PM emissions can be simulated from cycle to cycle by changing the vehicle running states, including the hot stabilized running state, idle running state, acceleration running state, hot start running state, and cold start running state. The hot stabilized running state refers the usual running state of the engine when the vehicle is moving on roads, which is the most frequent running state of vehicles in movement. With the rapid increase in vehicles in use, traffic congestion is growing and traffic jams during rush hours have become a common phenomenon in cities (Agarwal et al., 2015). Vehicles are frequently operated under the idle running state and hot start running state, in addition to the hot stabilized running state. Therefore, particles emitted under the idle running state and the hot start running state are also expected to be one of the major sources of PM, besides the emissions under the stabilized running state. The cold start refers to the stage of turning on the engine and the initial period of vehicle movement. The emissions in this stage contain more PM than those of other running states (May et al., 2014; Drozd et al., 2016), although the time of this state is usually very short.

The analyses of individual particles using transmission electron microscopes (TEM) and energy-dispersive X-ray detectors (EDX) can identify chemical compositions, internal inhomogeneity, mixing state and surface properties of individual particles, and have been widely used to characterize aerosol particles (Zhang et al., 1995; Li and Shao, 2009; Shao et al., 2017b). TEM has also been used to evaluate the soot nanostructure emitted from vehicles (Seong et al., 2014; Apicella et al., 2015; Weinbruch et al., 2016).

In this study, an experiment was conducted to evaluate the particles emitted from a PFI-engine vehicle. Emitted particles were collected under the states of cold start running, hot start running, hot stabilized running, acceleration running, and idle running. The particles were examined according to their morphologies, sizes and elemental composition identified using a TEM-EDX. The potential significance of the results for understanding the roles of vehicle emissions in urban air pollution is discussed.

1. Material and methods

1.1. Experimental vehicle, fuels, procedures, and sample collection

The PFI-engine vehicle was certified as compliant with China Phase 4 (equivalent to Euro 4) emission standards. Basic information about the vehicles is shown in Table 1. For the test vehicle, a three-way catalyst (TWC) was applied to reduce gaseous emissions. The test vehicle PFI-2.0-T was equipped with a 2.0-L PFI engine. Vehicles with this type of engine constitute the majority of vehicles in China, particularly in megacities like Beijing.

The fuel used had a Research Octane Number (RON) of 93 and Motor Octane Number (MON) of 84, and was a commercial gasoline blend of typical quality in China. The properties of the test fuel were measured by the SGS-CSTC Standards Technical Services Co., Ltd. in China, and are shown in Table 2. The fuel was a typical fifth-stage gasoline with high aromatics, which contained 36.7% aromatics, 15.4% olefins, and 6% sulfur by volume.

The experiments were conducted with a Beijing driving cycle (BDC), which was developed specifically to simulate the driving conditions in Beijing. The cycle included a 300-second start-up phase (cold start or hot start), followed by a 767-second hot stabilized running phase. The speed of the vehicle during the

Table 1 – Parameters for the vehicles in the experiment.	
Vehicle ID	PFI-2.0-T
Engine type	PFI
Induction system	turbo
Number of cylinders	4
Displacement (L)	1.799
Compression ratio	10.5
After-treatment	TWC
Bore (mm)	81.0
Stroke (mm)	87.3
Maximum power at engine speed /(kW/(r·min))	103/6300
Maximum torque at engine speed /((N·m)/(r·min))	174/4300

Table 2 – Properties of the fuels used in the experiment.	
Fuel	F1
RON	93
MON	84
Density (g/cm^3)	0.744
Aromatics (%, V/V)	36.7
Olefins (%, V/V)	15.4
EtOH (%, V/V)	0.01
Oxygen (%, m/m)	0.02
MMT (mg/L)	<1
Manganese (mg/kg)	<0.1
Sulfur (mg/kg)	6
T10 (°C)	55.4
T50 (°C)	109.9
T90 (°C)	164.3
FBP (°C)	194.4
FBP: final boiling point.	

and hot start BDC tests. After the fuel change and the BDC preparation, the vehicle was conditioned with an overnight soak. The soak-room temperature was controlled between 20 and 30°C. Before the cold start BDC, the difference between the temperature of the engine coolant and oil and the temperature of the soak was ensured less than 2°C. Because of the engine running time and the limitation of the facilities, the hot start tests were conducted within 5 min after the cold start test, and then similar hot start was conducted twice with 5-minute intervals.

The number concentration of particles during the tests was monitored by the Combustion Fast Particle Size Spectrometer DMS 500. The maximum measurable concentration of the DMS 500 was 10^{11} (dN/(dlogDp·cc)) while a diluter was used, and the uncertainty of the measurement was less than 7.5% (Petzold et al., 2011). A series of samples (6–8) for the individual particle analysis were collected during a BDC test. At least one sample was collected during each running state, including the cold start, hot start, idle state, acceleration state, and hot stabilized running state. The driving cycle test was repeated at least twice so that two or more samples were obtained for each running state.

A single-stage cascade impactor was mounted at the exit of the tailpipe to collect particles onto the carbon-sprayed formvar film on TEM grids (300-mesh copper) at a flow rate 1.0 L/min. The cut-off diameter of the impactor for the 50% collection efficiency was 0.25 μm for particles with the density of 2 g/cm^3. A dilution unit was applied to dilute the tailpipe

driving cycle is shown in Fig. 1a. The start-up phase consisted of starting the vehicle with a period of small acceleration, and the hot stabilized running phase had multiple periods of acceleration and deceleration with a maximum velocity of about 50 km/hr.

All experiments were carried out on a Euro 5/LEV2/Tier 2-capable climate controlled test unit on a 48-inch single-roll chassis dynamometer at Tsinghua University. The operation procedure for each test consisted of fuel change, BDC preparation, soaking for more than 10 hr overnight, cold start BDC tests,
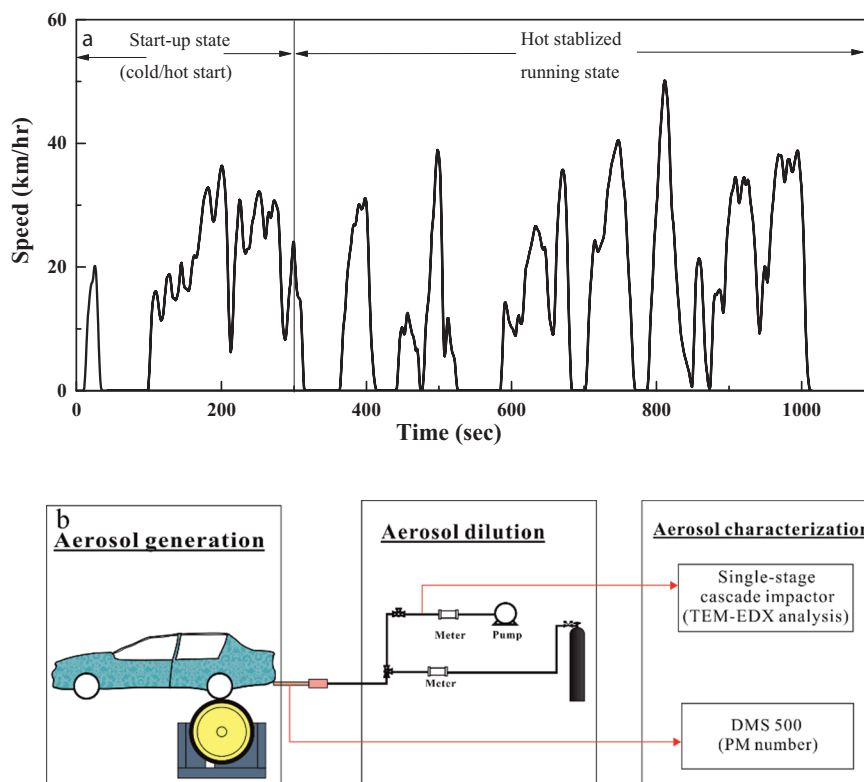

Fig. 1 – (a) Speed in one Beijing driving cycle under the running test. It is a cycle with a 300-sec "cold start" phase followed by a 767-sec "hot stabilized running" phase. (b) Sketch of the test system. The number concentration of particles during the tests was monitored by a Combustion Fast Particle Size Spectrometer DMS 500.

gas to 1/10 concentration using synthetic air composed of 79% N_2 and 20% O_2. For each sample, the collection time was 60 sec. The experimental system is illustrated in the following schematic diagram (Fig. 1b).

1.2. Sample analyses

The TEM grid samples were examined using the Tecnai G2 F30 TEM-EDX from the Beijing Center for Physical and Chemical Analysis. The TEM was operated at 300-kV acceleration voltage. In most cases, at least three micro-areas from each TEM grid were randomly chosen for the TEM-EDX analysis, and more than 150 particles in each sample were analyzed. The elemental composition of each individual particle larger than 50 nm in selected areas was analyzed using the EDX, which was able to semi-quantitatively detect elements heavier than carbon. EDX spectra were first collected for 20 live seconds to minimize possible influence of radiation exposure and potential beam damage, and then collected for 90 live seconds for a whole range of elements. Copper was excluded from the analysis because of interference from the copper TEM grids. The TEM images were digitized using an automated fringe image processing system to measure the projected areas of particles. The equivalent spherical diameter of a particle was calculated from its projected area, which was expressed as the square root of 4 A/π, where A is the projected area.

2. Results and discussion

2.1. Particle type, morphology, elemental composition and size distribution

TEM images of example particles are shown in Fig. 2. Most of the particles were in the size range of 300–1500 nm, covering the called accumulation mode size of aerosol particles. For particle classification, the method of Okada et al. (2005) and Xing et al. (2017) was used, and the results are shown in Fig. 2. "X-rich" means that the element "X" was rich and contributed the largest proportion among the elements in the particles (Okada et al., 2005).

Soot particles had chain-like and agglomerate shapes, and were consisted of up to several hundred carbon monomers (Fig. 2a). Carbon was the major element in the soot particles, and some soot particles contained Si, Zn, and Fe. Most of the soot aggregates were consisted of soot monomers only. Coating residues were not identified on the monomers or the aggregates from the TEM images.

Ca-rich particles had a spherical shape and contained Ca, P and O. Some of the particles contained Zn and Si (Fig. 2b). They were frequently in the size range of 300–500 nm and were relatively small in comparison with the mentioned soot particles. The spherical shape and small size indicated that the Ca-rich particles were condensed from elements in the

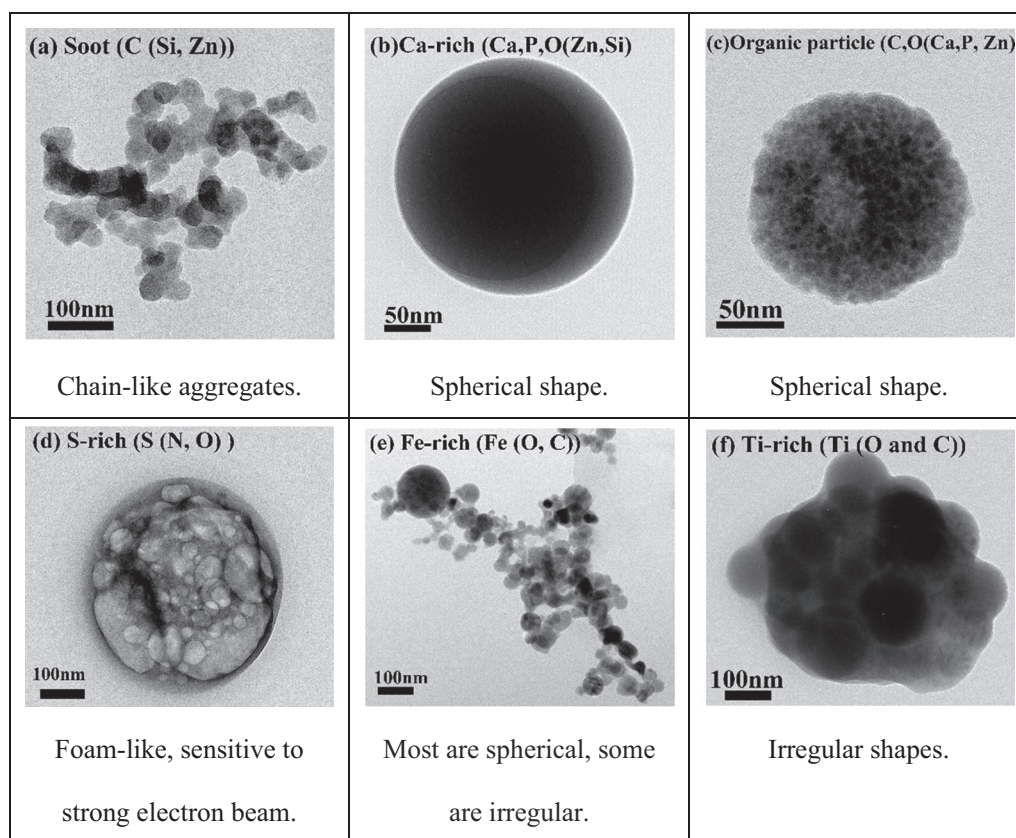| (a) Soot (C (Si, Zn))	(b) Ca-rich (Ca,P,O(Zn,Si)	(c) Organic particle (C,O(Ca,P, Zn)
100nm	50nm	50nm
Chain-like aggregates.	Spherical shape.	Spherical shape.
(d) S-rich (S (N, O))	(e) Fe-rich (Fe (O, C))	(f) Ti-rich (Ti (O and C))
100nm	100nm	100nm
Foam-like, sensitive to strong electron beam.	Most are spherical, some are irregular.	Irregular shapes.

Fig. 2 – TEM images and characteristics of particles from the vehicle. (a) Soot particles; (b) Ca-rich particles; (c) organic particles; (d) S-rich particles; (e) Fe-rich particles and (f) Ti-rich particles.

fuels or lubrication oil during the burning process (Rönkkö et al., 2014).

The organic particle is one of the spherical particles, and it belongs to the inhomogeneous carbonaceous organic particles with the sum of the C and lesser O content being higher than 60% (atomic fraction). Some other elements such as Ca, P, and Zn can also be found in organic particles (Fig. 2c). Previous studies reported that such particles could be related to the combustion of fuels or lubrication oil (Rönkkö et al., 2013). S-rich particles contained S, N and O, and rapidly decomposed under high-energy electron beam irradiation in the TEM, leaving S-rich residues (Fig. 2d). The formation of the S-rich particles was likely similar to the semi-volatile particles in diesel engine exhausts and directly depended on SO_2 conversion in the catalyst. (Arnold et al., 2012; Karjalainen et al., 2014a, 2014b). Metal-rich particles included Fe-rich and Ti-rich particles. Most of the Fe-rich particles were spherical (Fig. 2e) and were composed of O and C besides Fe. The Ti-rich particles had irregular shapes and contained Ti, O, and C (Fig. 2f).

In total, 2146 particles were analyzed. Organic particles, soot particles, and Ca-rich particles accounted for the major fractions, and there were a small amount of S-rich and metal-rich particles. Similar particle types were also found in gasoline engine bench tests, as well as in the emissions of heavy-duty diesel vehicles and in modern gasoline-fueled passenger vehicles (Rönkkö et al., 2014). Therefore, the particle types were not restricted to one vehicle type. They were common particle types in the emissions of both gasoline-fueled and diesel-fueled vehicles.

The dependence of number frequencies of particles on size is shown in Fig. 3. The particles were in the size range of 50–1500 nm and displayed a unimodal size distribution, with the peak at 600 nm. Similar results were also found in the gasoline engine bench tests (Xing et al., 2017) and a chassis dynamometer study (Lv et al., 2014). However, particles smaller than 250 nm might have been largely underestimated because of possible losses during particle collection.

2.2. Proportions of different particle types emitted under different running states

Running states had significant impacts on the PM emissions of vehicles, not only on the particle concentration, but also on the particle types and composition. Figure 4 illustrates the numbers of accumulation mode particles emitted by the burning of per unit of fuel under the cold start and hot start driving cycles. Moreover, the PM emissions at the start-up stages of both the cold start and the hot start running states were higher than the emissions at the states when the engine was fully warmed, and the vehicle operation was stabilized. The PM emissions were the highest under the cold start state, followed by those under the hot start, hot stabilized, and acceleration running states. The emissions were the lowest under the idle running state (Fig. 5).

The number fractions of different particle types in the emissions under different running states are shown in Fig. 6. The constitution of the emissions differed under the different running states. Soot particles were abundant in the emissions under the cold start running state. High number fractions of organic particles were found under the hot stabilized running state and the hot start running state. Relatively high number fractions of Ca-rich particles were found under the idle running state.

Soot particles accounted for more than 45% of the particles in the PM emissions under the cold start running state. A study by Bahreini et al. (2015) also demonstrated that the soot particle emissions from the vehicle under the cold start running state were significantly higher than the emissions under other running states. The production of the soot particles could be attributed to the incomplete volatilisation of fuel droplets in the piston and in the combustion cylinder (L. Chen et al., 2017). Fuel droplets that accumulated on the surface of combustion cylinders formed liquid pools, which favored soot formation, particularly at low temperatures (Xu et al., 2017). Moreover, the TWC could not efficiently oxidize the incomplete combustion products under the cold start
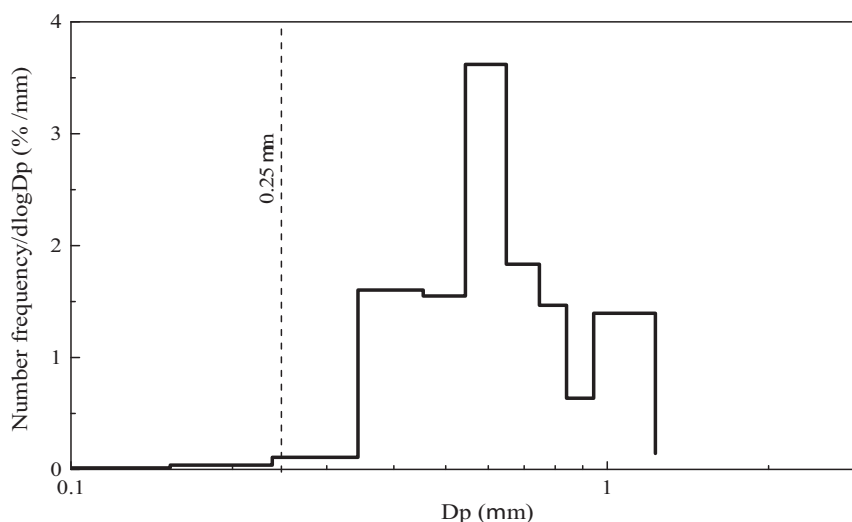
Fig. 3 – Number-size distribution of the particles emitted by the PFI-engine vehicle. Particles smaller than 0.25 μm should have been underestimated because of the collection efficiency of the impactor.
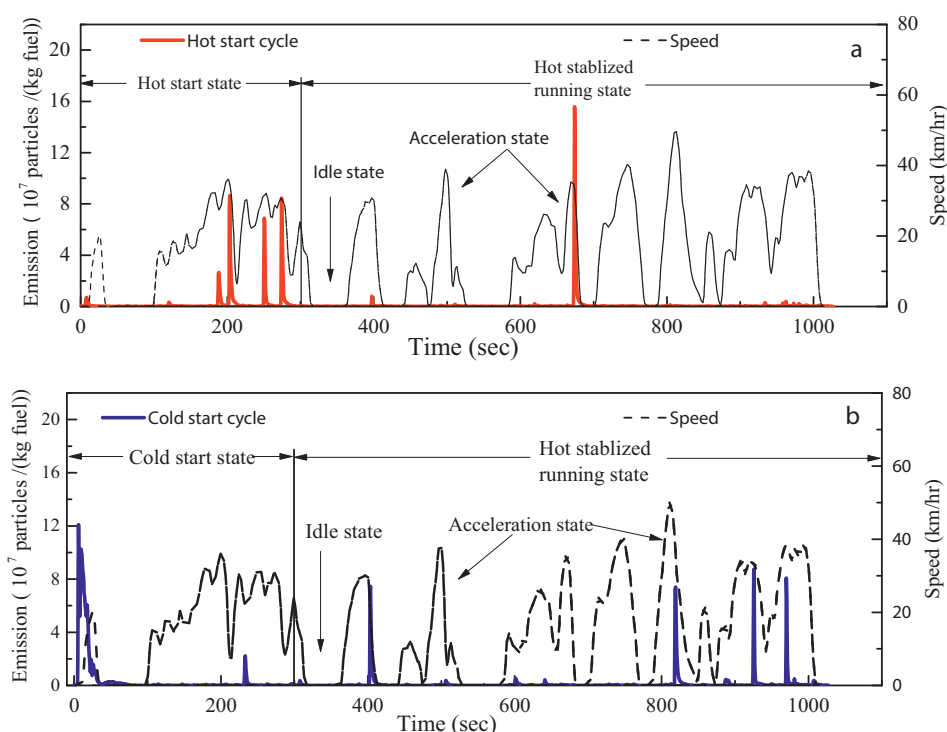
Fig. 4 – Particles in accumulation mode from the PFI-engine vehicle during hot start (a) and cold start (b) driving cycle. The vehicle speed is also shown for reference.

state when the temperature in the cylinders was lower than the light-off temperature (Mathis et al., 2005).

Under the hot start running state and the hot stabilized running state, organic particles predominated the PM emissions, accounting for more than 60% of the particles in the PM. Under these two running states, the engine temperature was high, which enabled the fuel to evaporate and mix with the air easily. The burning of the fuel was consequently close to complete burning, and the PM emissions under these two running states were lower than those under the cold start running state. With the increase in the temperature in the cylinders, the rate of particle oxidation was more efficient,

which led to an increase in the number of organic particles in the PM emissions (Fu et al., 2014).

Under the idle running state, the PM emissions were low, and Ca-rich particles were predominant. It was clear that the emissions and fuel consumption were significantly lower than those under other running states, because only a small amount of fuel was consumed to maintain engine operation. In other words, the contribution of lubricant oil to PM emissions was relatively higher than that of the oil under other running states. Previous studies have also shown that the distinctive characteristics of PM emissions under the idle running state are different from the emissions under other
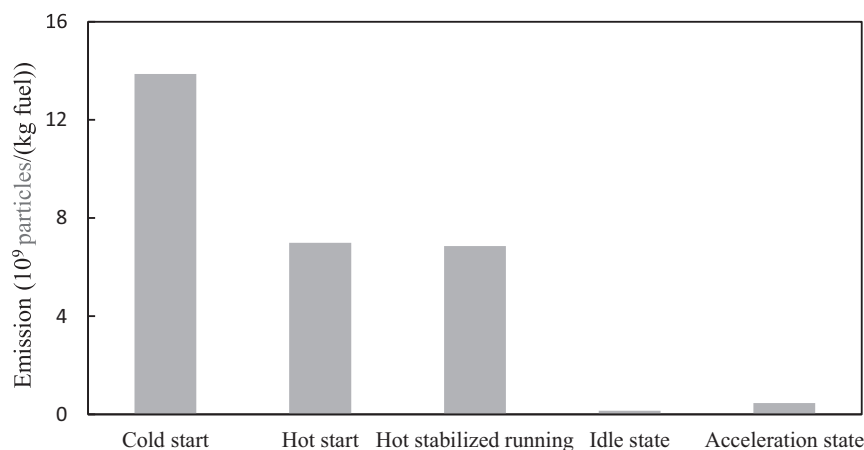

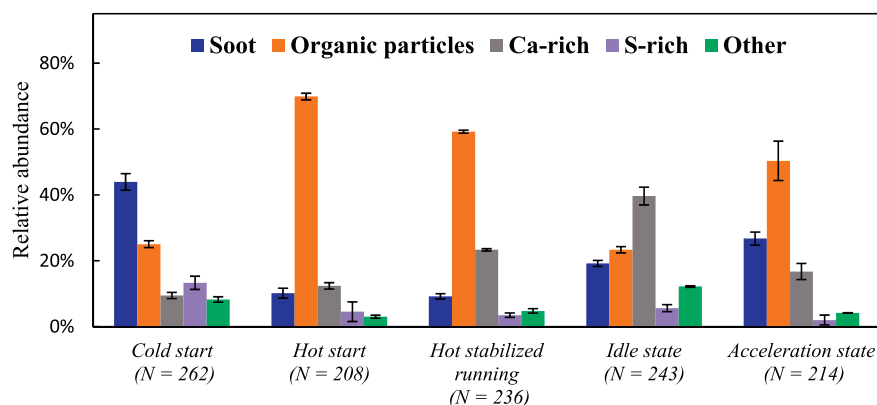Fig. 5 – Particles in accumulation mode from the PFI-engine vehicle under different running states.

Fig. 6 – Number fractions of different particle types in the emission of the PFI-engine vehicle under different running states. (*N* is the number of particles analyzed for the different running states).

running states (*e.g.*, Tong et al., 2000). Moreover, Lähde et al. (2014) reported that the particle emissions under the idle state were associated with the high content of Ca, and attributed the result to the influence of Ca content in the lubricant oil, which can also be confirmed by the present results (Fig. 6).

Under the acceleration running state, the PM emissions were lower than those of the other running states, except for the idle running state, and the predominant particle types included soot, organic, and Ca-rich particles. As the acceleration running state required high vehicular speed and engine load, the emissions contained more soot particles than those under other running states, in addition to the cold start running state.

We also estimated the number of different type particles in the emissions under the different running states by the burning of per unit of fuel (Fig. 7). The results showed that the emissions of organic particles were higher under the hot start running state (4.8×10^8 particles/(kg fuel)) and the hot stabilized running state (4.0×10^8 particles/(kg fuel)) than the emissions under other running states. The number of soot particles emitted from the vehicle by burning 1 kg of fuel was the highest under the cold start state (6.1×10^8). Under the idle running state, the relative number fraction of Ca-rich particles was the highest although their absolute number was low (0.6×10^7 particles/(kg fuel)).

2.3. Implications and perspectives

Vehicles with PFI engines are major sources of anthropogenic air pollutants in populated cities. Traffic emissions in cities like Beijing can constitute as much as 5%–31% of the $PM_{2.5}$ in pollution episodes (Y. Zhang et al., 2017). The present results show that the primary particles in the accumulation size range were organic particles (46% on average), soot particles (26%), Ca-rich particles (20%) and metal-rich particles such as Fe-rich and Ti-rich particles (Fig. 6).

After being emitted to the ambient environment, particles from traffic frequently undergo atmospheric aging and become internally mixed with secondary inorganic and organic aerosols (Yang et al., 2018). The particles from traffics could provide reaction sites for the formation of secondary aerosols (Niu et al., 2012; Peng et al., 2016). The mineral and metal components can enhance and catalyze the formation of sulfate, which is usually the largest secondary species in haze pollution (Hu et al., 2016; Hou et al., 2018). Therefore, it can be expected that the presence of the particles due to the emissions of PFI-engine vehicles can facilitate secondary aerosol formation *via* surface catalyzed reactions, as well as contribute inorganic and organic components as primary aerosols in the size range of the accumulation mode. To the extent of our knowledge, these subjects, *i.e.* the relative contributions of the processes and sources, have not
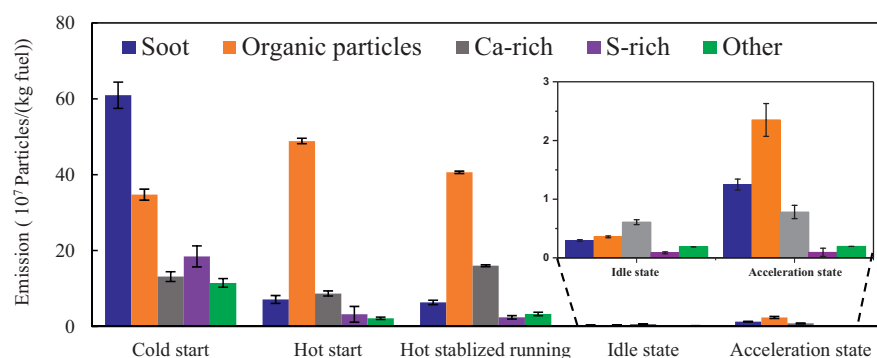

Fig. 7 – Number concentration of different particle types in the emission of the PFI-engine vehicle under different running states.

been addressed so far, which hinders a deep understanding on the roles that traffics play in populated urban atmospheric pollution.

Our results demonstrate that the concentrations of different particle types from the PFI-engine vehicle differed under different running states. Moreover, organic particles under the hot stabilized running state and the hot start running state were predominated by organic particles (Fig. 6). The number of organic particles under these two states could be up to 4.0×10^8 particles/(kg fuel) and 4.8×10^8 particles/(kg fuel), respectively (Fig. 7). Hot stabilized running is the most frequent running state of vehicles, and hot start running is the repeated running state of vehicles when they meet traffic jams. Therefore, substantial amounts of organic compounds in the air pollution in populated urban areas where frequent traffic jams occur might be directly related to vehicle emissions. In polluted urban atmospheres, the constitution of primary $PM_{2.5}$ particles are very complicated, with organic particles constituting up to 70% (S. Chen et al., 2017; Xu et al., 2017). Guo et al. (2012) demonstrated that the primary sources contributed more than 30% to the ambient organic carbon at an urban site. The gasoline vehicle sources are likely more important as they emit more organic particles.

The relative contents of Ca, P, and Zn in the organic particles from gasoline vehicle emissions were much higher than those from other sources (Liu et al., 2017). Similar to the present study, previous studies also showed the contents of Ca, P, K and Cl in individual particles, suggesting the relative ratios of the elements in air pollutants may provide potential fingerprints for the source apportionment of primary aerosols in ambient air (Weinbruch et al., 2018; J. Zhang et al., 2017). A source apportionment that more accurately quantifies organic compounds would be very beneficial to any new regulations for the control of $PM_{2.5}$ pollution.

Our results established an inventory of particle categories and amounts emitted from a PFI-engine vehicle under different running states (Fig. 7). With statistics on the number of vehicles with PFI engines, the running time and the running states on roads within a certain area, it is possible to get a rough estimate of the amount of different types of particles emitted from the vehicles. There are no similar data for the emissions from the vehicles with other types of engines, and we are currently unable, *via* inter comparisons, to quantitatively examine the significance of the vehicles with different types of engines as anthropogenic sources of primary particles. With the increase of more laboratory tests for the categories and relative amounts of particles from various vehicle engines coupling with filter-based analyses, it is ultimately possible to establish an inventory of particle categories and amounts emitted from different type vehicles. Studies on urban air pollution from process studies to pollution control strategies will largely benefit from such an inventory, which is the basis for the source apportioning of particles from vehicles.

3. Conclusions

1. Five types of particles in the emissions were identified, including soot, organic, Ca-rich, S-rich, and metal-rich particles, with the predominant types being organic particles (46%), soot (26%), and Ca-rich particles (20%). The particles were in the size range of 50–1500 nm and displayed a unimodal size distribution, with the peak at 600 nm.

2. The emissions were highest under the cold start state, followed by the hot start, hot stabilized, and acceleration running states. The PM emissions were lowest under the idle running state.

3. A high percentage of organic particles were emitted under the hot stabilized running state and hot start state, accounting for 70% and 59% of the PM, respectively. Soot particles were enriched in the emissions under the cold start state, accounting for 44% of the total particles. Ca-rich particles occupied the largest number fraction (40%) of particles under the idle running state.

4. Our results established an inventory of particle categories and amounts emitted from a PFI-engine vehicle under different running states. These results are largely beneficial to the source apportioning of particles from vehicles. In addition, the contents of Ca, P, and Zn in organic particles may serve as fingerprints for source apportionment of particles from PFI-engine vehicles.

REFERENCES

Agarwal, A.K., Gupta, T., Bothra, P., Shukla, P.C., 2015. Emission profiling of diesel and gasoline cars at a city traffic junction. Particuology 18, 186–193.

Apicella, B., Pré, P., Alfè, M., Ciajolo, A., Gargiulo, V., Russo, C., et al., 2015. Soot nanostructure evolution in premixed flames by high resolution electron transmission microscopy (HRTEM). Proc. Combust. Inst. 35 (2), 1895–1902.

Arnold, F., Pirjola, L., Ronkk, T., Reichl, U., Schlager, H., Lahde, T., et al., 2012. First online measurements of sulfuric acid gas in modern heavy-duty diesel engine exhaust: implications for nanoparticle formation. Environ. Sci. Technol. 46 (20), 11227–11234.

Arsie, I., Di Iorio, S., Vaccaro, S., 2013. Experimental investigation of the effects of AFR, spark advance and EGR on nanoparticle emissions in a PFI SI engine. J. Aerosol Sci. 64, 1–10.

Bahreini, R., Xue, J., Johnson, K., Durbin, T., Quiros, D., Hu, S., et al., 2015. Characterizing emissions and optical properties of particulate matter from PFI and GDI light-duty gasoline vehicles. J. Aerosol Sci. 90, 144–153.

Bond, T.C., Doherty, S.J., Fahey, D.W., Forster, P.M., Berntsen, T., Deangelo, B.J., et al., 2013. Bounding the role of black carbon in the climate system: a scientific assessment. J. Geophys. Res.-Atmos. 118 (11), 5380–5552.

California Air Resources Board (CARB), 2010. Preliminary discussion paper-proposed amendments to California's

low-emission vehicle regulations-particulate matter mass, ultra fine solid particle number, and black carbon emissions. Workshop Report.

Chart-Asa, C., Gibson, J.M., 2015. Health impact assessment of traffic-related air pollution at the urban project scale: influence of variability and uncertainty. Sci. Total Environ. 506, 409–421.

Chen, L., Liang, Z., Zhang, X., Shuai, S., 2017a. Characterizing particulate matter emissions from GDI and PFI vehicles under transient and cold start conditions. Fuel 189, 131–140.

Chen, S., Xu, L., Zhang, Y., Chen, B., Wang, X., Zhang, X., et al., 2017b. Direct observations of organic aerosols in common wintertime hazes in North China: insights into direct emissions from Chinese residential stoves. Atmos. Chem. Phys. 17 (2), 1259–1270.

Drozd, G.T., Zhao, Y., Saliba, G., Frodin, B., Maddox, C., Weber, R.J., et al., 2016. Time resolved measurements of speciated tailpipe emissions from motor vehicles: trends with emission control technology, cold start effects, and speciation. Environ. Sci. Technol. 50 (24), 13592–13599.

Fu, H., Wang, Y., Li, X., Shuai, S., 2014. Impacts of cold-start and gasoline RON on particulate emission from vehicles powered by GDI and PFI engines. SAE Technical Paper 2014-01-2836 https://doi.org/10.4271/2014-01-2836.

Guo, S., Hu, M., Guo, Q., Zhang, X., Zheng, M., Zheng, J., et al., 2012. Primary sources and secondary formation of organic aerosols in Beijing, China. Environ. Sci. Technol. (18), 9846–9853.

Hou, C., Shao, L., Hu, W., Zhang, D., Zhao, C., Xing, J., et al., 2018. Characteristics and aging of traffic-derived particles in a highway tunnel at a coastal city in southern China. Sci. Total Environ. 619-620, 1385–1393.

Hu, W., Niu, H., Zhang, D., Wu, Z., Chen, C., Wu, Y., et al., 2016. Insights into a dust event transported through Beijing in spring 2012: morphology, chemical composition and impact on surface aerosols. Sci. Total Environ. 565, 287–298.

Huang, R., Zhang, Y., Bozzetti, C., Ho, K., Cao, J., Han, Y., et al., 2014. High secondary aerosol contribution to particulate pollution during haze events in China. Nature 514 (7521), 218–222.

Jakober, C.A., Robert, M.A., Riddle, S.G., Destaillats, H., Charles, M.J., Green, P.G., et al., 2008. Carbonyl emissions from gasoline and diesel motor vehicles. Environ. Sci. Technol. 42 (13), 4697–4703.

Karavalakis, G., Short, D., Vu, D., Russell, R., Hajbabaei, M., Asa-Awuku, A., et al., 2015. Evaluating the effects of aromatics content in gasoline on gaseous and particulate matter emissions from SI-PFI and SIDI vehicles. Environ. Sci. Technol. 49 (11), 7021–7031.

Karjalainen, P., Pirjola, L., Heikkilä, J., Lähde, T., Tzamkiozis, T., Ntziachristos, L., et al., 2014a. Exhaust particles of modern gasoline vehicles: a laboratory and an on-road study. Atmos. Environ. 97, 262–270.

Karjalainen, P., Ronkko, T., Pirjola, L., Heikkila, J., Happonen, M., Arnold, F., et al., 2014b. Sulfur driven nucleation mode formation in diesel exhaust under transient driving conditions. Environ. Sci. Technol. 48 (4), 2336–2343.

Lähde, T., Virtanen, A., Happonen, M., Söderström, C., Kytö, M., et al., 2014. Heavy-duty, off-road diesel engine low-load particle number emissions and particle control. J. Air Waste Manage. Assoc. 64 (10), 1186–1194.

Leach, F., Stone, R., Richardson, D., 2013. The influence of fuel properties on particulate number emissions from a direct injection spark ignition engine. SAE Technical Paper 2013-01-1558 https://doi.org/10.4271/2013-01-1558.

Li, W., Shao, L., 2009. Transmission electron microscopy study of aerosol particles from the brown hazes in northern China. J. Geophys. Res.-Atmos. https://doi.org/10.1029/2008JD011285.

Liu, Z.G., Vasys, V.N., Kittelson, D.B., 2007. Nuclei-mode particulate emissions and their response to fuel sulfur content and primary dilution during transient operations of old and modern diesel engines. Environ. Sci. Technol. 41 (18), 647–6483.

Liu, L., Kong, S., Zhang, Y., Wang, Y., Xu, L., Yan, Q., et al., 2017. Morphology, composition, and mixing state of primary particles from combustion sources - crop residue, wood, and solid waste. Sci. Rep. https://doi.org/10.1038/s41598-017-05357-2.

Lv, G., Song, C., Pan, S., Gao, J., Cao, X., 2014. Comparison of number, surface area and volume distributions of particles emitted from a multipoint port fuel injection car and a gasoline direct injection car. Atmos. Pollut. Res. 5 (4), 753–758.

Mathis, U., Mohr, M., Forss, A., 2005. Comprehensive particle characterization of modern gasoline and diesel passenger cars at low ambient temperatures. Atmos. Environ. 39 (1), 107–117.

May, A.A., Nguyen, N.T., Presto, A.A., Gordon, T.D., Lipsky, E.M., Karve, M., et al., 2014. Gas- and particle-phase primary emissions from in-use, on-road gasoline and diesel vehicles. Atmos. Environ. 88, 247–260.

Myung, C.L., Park, S., 2012. Exhaust nanoparticle emission from internal combustion engines: a review. Int. J. Automot. Technol. 1 (13), 9–22.

National Bureau of Statistics of China, 2015. China statistical yearbook 2015, part eighteen: transportation, post and telecommunications and software industry. Available online at http://www.stats.gov.cn/tjsj/ndsj/2015/indexch.htm.

Niu, H., Shao, L., Zhang, D., 2012. Soot particles at an elevated site in eastern China during the passage of a strong cyclone. Sci. Total Environ. 430, 217–222.

Okada, K., Qin, Y., Kai, K., 2005. Elemental composition and mixing properties of atmospheric mineral particles collected in Hohhot, China. Atmos. Res. 73, 45–67.

Peng, J., Hu, M., Guo, S., Du, Z., Zheng, J., Shang, D., et al., 2016. Markedly enhanced absorption and direct radiative forcing of black carbon under polluted urban environments. Proc. Natl. Acad. Sci. U. S. A. 113, 4266–4271.

Petzold, A., Marsh, R., Johnson, M., Miller, M., Sevcenco, Y., Delhaye, D., et al., 2011. Evaluation of methods for measuring particulate matter emissions from gas turbines. Environ. Sci. Technol. 45 (8), 3562–3568.

Rönkkö, T., Lähde, T., Heikkilä, J., Pirjola, L., Bauschke, U., Arnold, F., et al., 2013. Effects of gaseous sulphuric acid on diesel exhaust nanoparticle formation and characteristics. Environ. Sci. Technol. 47, 11882–11889.

Rönkkö, T., Pirjola, L., Ntziachristos, L., Heikkilä, J., Karjalainen, P., Hillamo, R., et al., 2014. Vehicle engines produce exhaust nanoparticles even when not fueled. Environ. Sci. Technol. 48 (3), 2043–2050.

Seong, H., Choi, S., Lee, K., 2014. Examination of nanoparticles from gasoline direct-injection (GDI) engine using transmission electron microscopy (TEM). Int. J. Automot. Technol. 15 (2), 175–181.

Shao, L., Hu, Y., Fan, J., Wang, J., Wang, J., Ma, J., 2017a. Physicochemical characteristics of aerosol particles in the Tibetan Plateau: Insights from TEM-EDX analysis. J. Nanosci. Nanotechnol. 17 (9), 6899–6908.

Shao, L., Hu, Y., Shen, R., Schäfer, K., Wang, J., Wang, J., et al., 2017b. Seasonal variation of particle-induced oxidative potential of airborne particulate matter in Beijing. Sci. Total Environ. 579, 1152–1160.

Tong, H.Y., Hung, W.T., Cheung, C.S., 2000. On-road motor vehicle emissions and fuel consumption in urban driving conditions. J. Air Waste Manage. Assoc. 50 (4), 543–554.

Weinbruch, S., Benker, N., Kandler, K., Ebert, M., Ellingsen, D.G., Berlinger, B., et al., 2016. Morphology, chemical composition and nanostructure of single carbon-rich particles studied by transmission electron microscopy: source apportionment in workroom air of aluminium smelters. Anal. Bioanal. Chem. 408 (4), 1151–1158.

Weinbruch, S., Benker, N., Kandler, K., Schuetze, K., Kling, K., Berlinger, B., et al., 2018. Source identification of individual

soot agglomerates in Arctic air by transmission electron microscopy. Atmos. Environ. 172, 47–54.

Xing, J., Shao, L., Zheng, R., Peng, J., Wang, W., Guo, Q., et al., 2017. Individual particles emitted from gasoline engines: impact of engine types, engine loads and fuel components. J. Clean. Prod. 149, 461–471.

Xu, L., Liu, L., Zhang, J., Zhang, Y., Ren, Y., Wang, X., et al., 2017. Morphology, composition, and mixing state of individual aerosol particles in Northeast China during wintertime. Atmosphere 8 (3), 47.

Yang, B., Ma, P., Shu, J., Zhang, P., Huang, J., Zhang, H., 2018. Formation mechanism of secondary organic aerosol from ozonolysis of gasoline vehicle exhaust. Environ. Pollut. 234, 960–968.

Yu, L., Wang, G., Zhang, R., Zhang, L., Song, Y., Wu, B., et al., 2013. Characterization and source apportionment of PM$_{2.5}$ in an urban environment in Beijing. Aerosol Air Qual. Res. 13 (2), 574–583.

Zhang, D., Tang, X., Qin, Y., Iwasaka, Y., Gai, X., 1995. Tests for individual sulfate-containing particles in urban atmosphere in Beijing. Adv. Atmos. Sci. 12, 343–350.

Zhang, Y., Cai, J., Wang, S., He, K., Zheng, M., 2017a. Review of receptor-based source apportionment research of fine particulate matter and its challenges in China. Sci. Total Environ. 586, 917–929.

Zhang, J., Liu, L., Wang, Y., Ren, Y., Wang, X., Shi, Z., et al., 2017b. Chemical composition, source, and process of urban aerosols during winter haze formation in Northeast China. Environ. Pollut. 231, 357–366.

Zhu, R., Hu, J., Bao, X., He, L., Lai, Y., Zu, L., et al., 2016. Tailpipe emissions from gasoline direct injection (GDI) and port fuel injection (PFI) vehicles at both low and high ambient temperatures. Environ. Pollut. 216, 223–234.